processes

MDPI

Article

An Optimization Method for an Integrated Energy System Scheduling Process Based on NSGA-II Improved by Tent Mapping Chaotic Algorithms

Shengran Chen [1] and Shengyan Wang [2,*]

[1] Dongguan Power Supply Company of Guangdong Province, Dongguan 523000, China, chenshengran@gddg.csg.cn
[2] North China Electric Power University, Beijing 102206, China
* Correspondence: 1182206089@ncepu.edu.cn; Tel.: +86-178-1212-1995

Received: 24 January 2020; Accepted: 23 March 2020; Published: 3 April 2020

Abstract: The integrated energy system is a vital part of distributed energy industries. In addition to this, the optimal economic dispatch model, which takes into account the complementary coordination of multienergy, is an important research topic. Considering the constraints of power balance, energy supply equipment, and energy storage equipment, a basic model of optimal economic dispatch of an integrated energy system is established. On this basis, a multiobjective function solving algorithm of NSGA-II, based on tent map chaos optimization, is proposed. The proposed model and algorithm are applied. The simulation results show that the optimal economic scheduling model of the integrated energy system established in this paper can provide a more economic system operation scheme and reduce the operation cost and risks associated with an integrated energy system. The Non-dominated Sorting Genetic Algorithm-II (NSGA-II) multiobjective function solving algorithm, based on tent map chaos optimization, has better performance and efficiency.

Keywords: integrated energy system; optimal economic dispatch; tent map; chaotic optimization

1. Introduction

With the increasing demand for energy, the integrated energy system, as a key component of the energy internet, can form a unified and efficient energy management platform that includes power networks, thermal networks, and natural gas networks [1–3]. Integrated energy systems interconnect different forms of energy networks through energy-coupling devices, such as Combined Cooling Heating and Power (CCHP) units, gas-to-electricity devices, and fuel cells, to achieve multienergy complementary coordination [4,5]. At the same time, energy storage devices optimize the allocation of energy in the time dimension, which can reduce the integrated operation cost of the system while meeting the requirements of energy supply; therefore, making the system more economical.

As one of the key technical problems, the optimal economic dispatch model of the integrated energy system has been researched in many studies. On the one hand, these studies establish more objective and reasonable economic dispatching models, such as the regional integrated energy system optimal economic dispatching model with a power network as the core in reference [6]. Gu Wei et al. [7] established a mixed integer linear programming economic dispatching model for a multidistrict integrated energy system based on the operation principle of the CCHP system; Shi Jinyue et al. [8] established an optimal operation model for an integrated energy system using two-level programming theory. Other studies have focused on model solving algorithms. For example, in reference [9], the Benders decomposition algorithm is used to solve the model. Zhou Canhuang et al. [10] used particle swarm optimization algorithm to solve the optimal operation model of the integrated energy

system of the campus microgrid. Zhang Xia et al. [11] present a reliability evaluation algorithm for a regional integrated energy system based on the particle swarm optimization (PSO) interior point hybrid optimization algorithm, which can effectively evaluate the effect of the optimal operation of an integrated energy system. Lin Wei et al. [12] solved the mixed power flow algorithm of the regional integrated energy system through multiobjective optimization, and then obtained the optimized operation plan of the system. However, as basic algorithms, the above algorithms have limited potential in further improving the performance of model solving. At present, few papers use the Non-Dominated Sorting Genetic Algorithm-II (NSGA-II) multiobjective function solving algorithm based on tent map chaos optimization to design the solving process for the economic dispatch model of an integrated energy system.

Firstly, aiming at the multienergy complementary coordination characteristics in the optimization of economic dispatch of an integrated energy system, the optimal economic dispatch model of an integrated energy system is established in this study. On this basis, the objective function is solved by using the tent map chaotic optimization NSGA-II algorithm. Although the traditional NSGA-II algorithm has been widely used in the field of multiobjective optimization, it still has the problem of local optimization. In this paper, the chaotic optimization algorithm of the tent map is embedded in the main flow of the NSGA-II algorithm. By improving the initialization process and elite retention process of the algorithm, the search space is enlarged, the algorithm is prevented from falling into local optimization, and the convergence speed of the algorithm is accelerated. It enhances the computational efficiency, robustness, and applicability of the algorithm, and ultimately, improves the performance of solving the multiobjective optimization model. Finally, the algorithm is used to verify the effectiveness of the model and the tent map chaos optimization NSGA-II algorithm.

2. Economic Dispatch model of Integrated Energy System

2.1. Objective Function

The integrated energy system is composed of different forms of energy networks; hence, the control variables of its economic dispatch model include the equipment operation plans of different forms of energy. The objective function of economic dispatch of an integrated energy system is to minimize the daily operating cost of the system, as shown in Equation (1).

$$C = C_1 + C_2 + C_3 + C_4 \tag{1}$$

where C is the daily operating cost of an integrated energy system; C_1 is the operating cost of an electrical power network; C_2 is the operation cost of a thermal energy network; C_3 is the operation cost of a gas energy network; and C_4 is the operation cost of an electric vehicle charging station network.

$$\min C_1 = \sum_{t=1}^{T}\left[P_{\text{grid}}(t)q_{\text{grid}}(t) + k_{\text{SB}}\left|P_{\text{SB}}(t)\right| + k_{\text{WT}}P_{\text{WT}}(t) + k_{\text{PV}}P_{\text{PV}}(t) + \beta q_{\text{grid}}(t)P_{\text{cut}}(t)\right] \tag{2}$$

where $P_{\text{grid}}(t)$ is the t-period exchange power between the public coupling point of the power network and the external network; $q_{\text{grid}}(t)$ is the time-sharing price level of the external network for t-period; $P_{\text{WT}}(t)$ is the wind power output for t-period; $P_{\text{PV}}(t)$ is the photovoltaic power output for t-period; k_{SB}, k_{WT}, and k_{PV} are energy storage, wind power, and the photovoltaic operation cost coefficient—they are all constants; $P_{\text{SB}}(t)$ is the charging and discharging power for t-period energy storage; β is the interruption compensation coefficient; and $P_{\text{cut}}(t)$ is the load interruption capacity of the t-period.

$$\min C_2 = \sum_{t=1}^{T}\left[\frac{P_{\text{MT}}(t)C_{\text{NG}}}{\eta_{\text{MT}}(t)Q_{\text{LHV}}} + P_{\text{H}}(t)p_{\text{h}}(t) + \sum_{\theta=1}^{N}\lambda_{\text{MT}}^{\theta}c^{\theta}\left(\frac{P_{\text{MT}}(t)}{\eta_{\text{MT}}(t)} - P_{\text{MT}}(t)\right)\right] \tag{3}$$

where $P_{MT}(t)$ is the heating power of a microgas turbine with t-period combined cooling, heating, and power supply, i.e., the energy input of a dual-effect absorption unit; $\eta_{MT}(t)$ is the thermal efficiency of the t-period combined cooling, heating, and power microcombustor; C_{NG} is the unit price of natural gas; Q_{LHV} is the low calorific value of natural gas; $P_H(t)$ is the purchasing power of the t-period thermal energy network; $p_h(t)$ is the heating price of the t-period thermal energy network; θ is the pollutant category, and there are N pollutants; λ_{MT}^{θ} is the emission coefficient of the θth pollutant, which is a constant; and c^{θ} is the unit emission control cost of the θth pollutant, which is also a constant.

$$\min C_3 = \sum_{t=1}^{T}\left[Q_{in}(t)C_{NG} + \sum_{\theta=1}^{N}\lambda_{FC}^{\theta}c^{\theta}P_{FC}(t)\right] \tag{4}$$

where $Q_{in}(t)$ is the intake volume of a gas source point for t-period; λ_{FC}^{θ} is the emission coefficient of the θth pollutant; and $P_{FC}(t)$ is the power generation of a fuel cell for t-period.

$$\min C_4 = \sum_{i=1}^{N}\sum_{t=1}^{T}P_{grid}(t)P_i(t) \tag{5}$$

where $P_i(t)$ is the charging load power of the charging station of the i electric vehicle in t-period.

2.2. Constraint Condition

2.2.1. Energy Power Balance Constraints in Various Forms

The constraints include energy balance constraints, thermal energy balance constraints, and gas energy balance constraints, as shown in Equations (6), (8), and (9), respectively.

$$P_{grid}(t) + P_{MT}(t) + P_{FC}(t) + P_{WT}(t) + P_{PV}(t) + P_{SB}(t) = P_L(t) + P_{loss}(t) + P_G(t) \tag{6}$$

where $P_L(t)$ is the load power of the t-period electric power subnet and $P_{loss}(t)$ is the loss power of the t-period power subnet. The calculation method is shown in Equation (7). $P_G(t)$ is the electric switching power for the t-period power subnet, which was realized by methane switching equipment.

$$P_{loss}(t) = \sum_{k=1}^{M}\frac{P_k^2 + Q_k^2}{U_k^2}R_k \tag{7}$$

where P_k and Q_k are the active and reactive power for branch k; M is the number of branches in the power electronic network; R_k is the resistance of branch k; and U_k is the rated voltage of the branch k.

$$P_{MT}(t)C_{he} + V_x(t) + P_H(t) = L_{he}(t) \tag{8}$$

where C_{he} is the heating coefficient of the double-effect absorption unit; $L_{he}(t)$ is the heat load of the t-period heat energy subnetwork; $V_x(t)$ is the heat stored in the t-period energy storage device, which is stored when it is greater than zero, and released when it is less than zero; and $P_H(t)$ is the heating power of the t-period heat energy external network relative to the heat subnetwork.

$$Q_{in}(t) + P_G(t) = \frac{P_{FC}(t)}{\eta_{FC}(t)Q_{LHV}} + \frac{P_{MT}(t)}{\eta_{MT}(t)Q_{LHV}} + L_g(t) \tag{9}$$

where $L_g(t)$ is the gas load of the t-period and η_{FC} and η_{MT} represent the efficiency of the fuel cell and the efficiency of the microturbine, respectively.

2.2.2. Operation Constraints of Energy Supply Equipment

The constraint is shown in Equation (10).

$$\begin{cases} P_{\text{grid}}^{\min} \le P_{\text{grid}}(t) \le P_{\text{grid}}^{\max} \\ P_{\text{H}}^{\min} \le P_{\text{H}}(t) \le P_{\text{H}}^{\max} \\ 0 \le P_{\text{FC}}(t) \le P_{\text{FC}}^{\max} \\ 0 \le Q_{\text{in}}(t) \le Q_{\text{in}}^{\max} \\ 0 \le P_{\text{MT}}(t) \le P_{\text{MT}}^{\max} \end{cases} \tag{10}$$

where $P_{\text{grid}}^{\min}$ and $P_{\text{grid}}^{\max}$ are the minimum and maximum switching power between the power subnet and the external network, respectively; $P_{\text{H}}^{\min}$ and $P_{\text{H}}^{\max}$ are the minimum heating power and the maximum heating power of the heat energy external network, respectively; $Q_{\text{in}}^{\max}$ is the air intake at the maximum resource point for a gas energy subnet; $P_{\text{FC}}^{\max}$ is the output limit of fuel cells; and $P_{MT}^{\max}$ is the output limit of the microturbine for CCHP.

2.2.3. Operation Constraints of Energy Storage Equipment

The constraint is shown in Equation (11).

$$\begin{cases} P_{\text{SB}}^{\min} \le P_{\text{SB}}(t) \le P_{\text{SB}}^{\max} \\ S_{\text{SB}}^{\min} \le S_{\text{SB}}(t) \le S_{\text{SB}}^{\max} \\ S_{\text{SB}}(t+1) = \\ \begin{cases} S_{\text{SB}}(t) - P_{\text{SB}}(t)\Delta t/\eta_{\text{dis}} - \Delta t D_{\text{SB}} Q_{\text{SB}}, P_{\text{SB}}(t) > 0 \\ S_{\text{SB}}(t) - P_{\text{SB}}(t)\Delta t \eta_{\text{ch}} - \Delta t D_{\text{SB}} Q_{\text{SB}}, P_{\text{SB}}(t) < 0 \end{cases} \\ X(t) = X(t-1) + V_x(t) - \lambda_x \Delta t \\ V_{\min} \le V_{\text{x}}(t) \le V_{\max} \\ X_{\min} \le X(t) \le X_{\max} \\ Q_s(t) = Q_s(t-1) + G_s(t) \\ G_s^{\min} \le G_s(t) \le G_s^{\max} \\ Q_s^{\min} \le Q_s(t) \le Q_s^{\max} \end{cases} \tag{11}$$

where $P_{\text{SB}}^{\min}$ and $P_{\text{SB}}^{\max}$ are the minimum and maximum energy storage output, respectively; $S_{\text{SB}}(t)$ and $S_{\text{SB}}(t+1)$ are storage battery (SB) residual electricity at the end of the t-period and the $t+1$-period; η_{dis} is the SB discharge efficiency; η_{ch} is the SB charging efficiency; $\text{S}_{\text{SB}}^{\min}$ and $\text{S}_{\text{SB}}^{\max}$ are the minimum and maximum energy storage residual electricity, respectively; Δt is the time interval; D_{SB} is the energy storage self-discharge coefficient; Q_{SB} is the energy storage capacity; $X(t)$ is the remaining heat (cooling capacity) of the t-period energy storage device; $X(t-1)$ is the remaining heat (cooling capacity) of the $t-1$-period energy storage device; λ_x is the self-loss coefficient of the remaining heat (cooling capacity) for the energy storage device; $V_x(t)$ is the charging and discharging power of the t-period; $V_{\min}$ and $V_{\max}$ are the minimum and maximum of the charging and discharging power of the energy storage device, respectively; $X_{\min}$ and $X_{\max}$ are the minimum and maximum of the residual heat of the energy storage device, respectively; $Q_s(t)$ and $Q_s(t-1)$ are the gas remains of gas storage tanks of the t-period and $t+1$-period, respectively; $G_s(t)$ is the gas release from a gas storage tank of the t-period; $Q_s^{\min}$ and $Q_s^{\max}$ are the minimum and maximum gas residue of the gas storage tank, respectively; and $G_s^{\min}$ and $G_s^{\max}$ are the minimum and maximum gas release from the gas storage tank, respectively.

2.2.4. Other Operational Constraints

Other operational constraints are shown in Equation (12).

$$0 \le P_{\text{cut}}(t) \le P_{\text{cut}}^{\max} \tag{12}$$

where P_{cut}^{max} is the interruptible load capacity for integrated energy systems signed with users.

3. NSGA-II Optimization Algorithm Based on Tent Mapping Chaos

The objective function constructed in this paper is a multiobjective optimization problem. Therefore, the NSGA-II algorithm, which is widely used in the field of multiobjective optimization, is introduced, and the chaotic optimization algorithm is applied to improve its adaptability in order to achieve a better solution of the model.

3.1. NSGA-II Algorithm

NSGA-II is a classical multiobjective genetic algorithm, which introduces the fast non-dominant ranking method and elite strategy, defines the crowding degree instead of adaptive value sharing, reduces the computational complexity of the algorithm, and improves the computational efficiency. If there are N subgoals, NSGA-II defines the crowding degree of individual i as follows:

$$P(i) = \sum_{k=1}^{N} \left| x_k(i+1) - x_k(i-1) \right| \tag{13}$$

In Equation (13), $x_k(i+1)$ and $x_k(i-1)$ are the optimal values of $i+1$ and $i-1$ individuals in the k target, respectively. The detailed calculation process of the traditional NSGA-II algorithm is shown in the literature [13].

3.2. Chaos Optimization Algorithm for Tent Mapping

Chaotic optimization's purpose is to map optimization variables to the value interval of chaotic variable space through chaotic mapping rules. By using ergodicity and a regularity search of chaotic variables, the optimization solution is linearly transformed into an optimization space [14]. Logistic mapping is usually used. However, recent related studies show that tent mapping has better chaotic characteristics than logistic mapping [15]. The improved tent map is shown in Equation (15).

$$\begin{cases} x_{k+1} = T(x_k) + 0.1 \times rand(0,\ 1) & x_k = 0,\ 0.25,\ 0.5,\ 0.75\ or\ x_k = x_{k-m} \\ x_{k+1} = T(x_k) & else \end{cases} \tag{14}$$

Among them,

$$T(x_k) = \begin{cases} 2x_k & 0 \le x_k \le 0.5 \\ 2(1 - x_k) & 0.5 < x_k \le 1 \end{cases} \tag{15}$$

3.3. Combination Algorithm Flow and Steps

Although NSGA-II has been widely used in the field of multiobjective optimization, there are still significant local optimization problems [16]. This is because the elite strategy gives the local optimal solution too much genetic advantage in the later iteration of the algorithm, which limits the algorithm's ability to further search for a wider or better region. At the same time, the initialization process of the algorithm uses entirely random values, which possibly causes the multipeak function to have a blind search area [17]. In this paper, an improved NSGA-II algorithm was proposed. The chaotic optimization algorithm based on tent mapping is embedded in the main flow of the NSGA-II algorithm. By improving the initialization process and elite retention process of the algorithm, on the one hand, the convergence speed of the algorithm is accelerated, and the efficiency of the initial optimization of the algorithm can be improved; on the other hand, the search space can be enlarged, and the genetic advantage of the elite strategy can be weakened at the later stage of the algorithm. The advantages of the algorithm make it possible to escape the local optimum and increase the probability of obtaining the global optimal solution. At the same time, the improvement process strengthens the robustness of the algorithm, expands the applicability of the algorithm, and ultimately, improves the optimization

performance of the algorithm as a whole. The flow chart of chaotic optimization NSGA-II algorithm based on the tent map is shown in Figure 1.

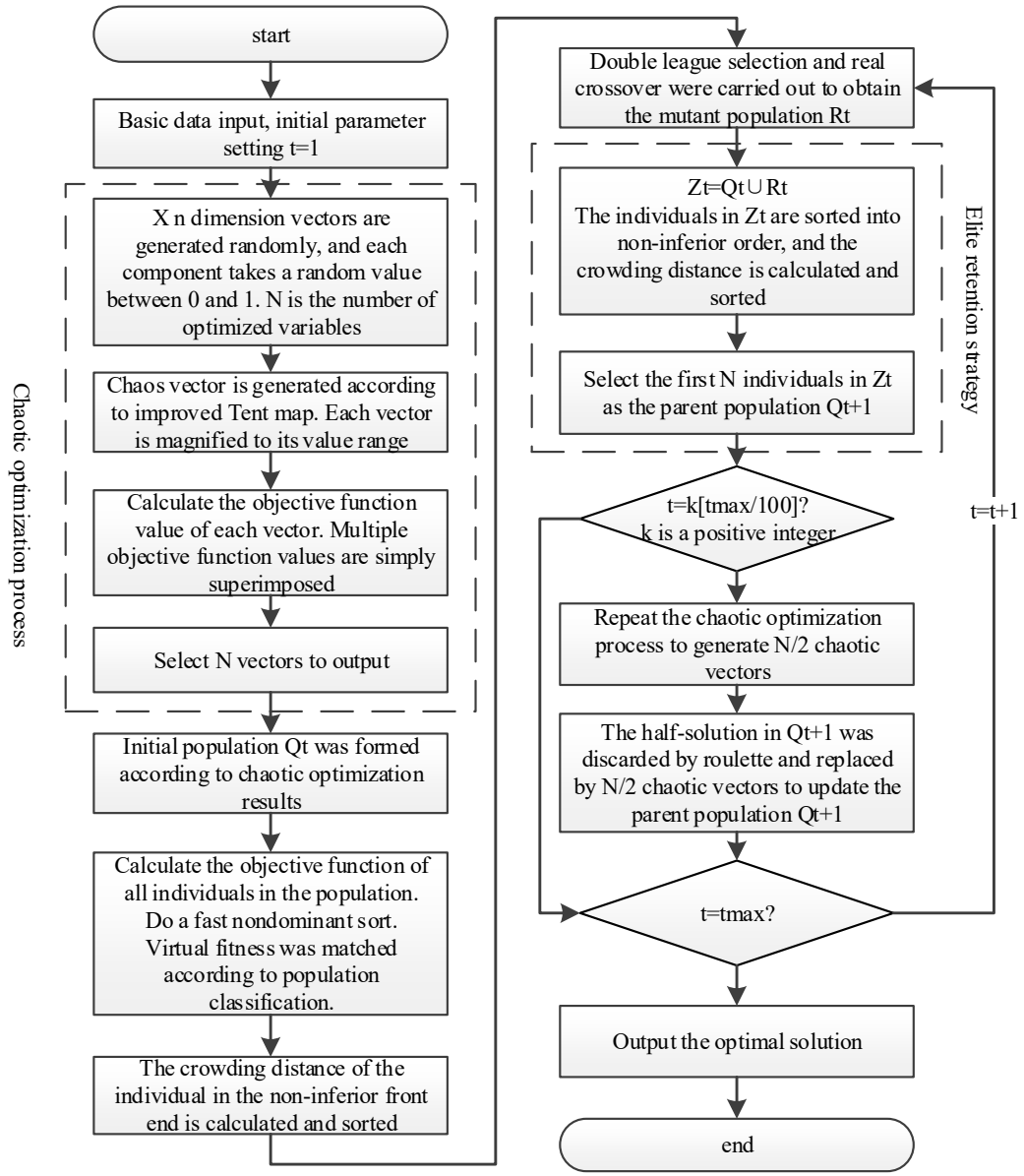

Figure 1. Flow chart of the Non-Dominated Sorting Genetic Algorithm-II (NSGA-II) algorithm based on tent mapping.

4. Numerical Example

Taking the demonstration project of an intelligent integrated energy system in Tayuanzhuang, Hebei Province in China as an example, this paper uses its own established model to design the system operation. In the optimized economic dispatching model, the unit price of natural gas C_{NG} is 0.29 USD/m^3; the dispatching period of the system is 1 h, the load interruption compensation coefficient β is 3; the discharge efficiency η_{dis} and charging efficiency η_{ch} of energy storage are both 0.87; the self-discharge coefficient of energy storage D_{SB} is 0.1, and the storage capacity Q_{SB} is 1000 kWh; the self-loss coefficient of the residual heat (cooling capacity) of the energy storage device λ_x is 0.1; the capacity of the gas storage tank Q_s^{max} is 400 m^3. The conversion cost of pollutants and emission factors and the time-of-use tariff mechanism for external networks are shown in Tables 1 and 2, respectively. In the demonstration project of the Tayuanzhuang Intelligent Integrated Energy System, the allocation

capacity of the CCHP unit, fuel cell, photovoltaic power generation, wind power generation, battery energy storage, dual-effect absorption unit, energy storage device, and methane-type converter unit are 500 kW, 200 kW, 500 kW, 300 kW, 250 kW, 300 kW, 200 kW, and 300 kW, respectively.

Table 1. Conversion costs of pollutants and emission factors.

Type of Pollutant	Conversion Cost (USD/kg)	MT Emission Factor (kg/kW)	FC Emission Factor (kg/kW)
NO_x	3.78	4.4×10^{-4}	4.5×10^{-6}
SO_2	0.89	8.0×10^{-6}	2.25×10^{-6}
CO_2	0.01	1.6×10^{-3}	4.27×10^{-3}

Table 2. Time-of-use tariff mechanism for external networks.

Time Slot Type	Time Slot	Electricity Price (USD/kWh)
Peak time	10:00–15:00 and 18:00–21:00	0.12
Valley time	00:00–07:00 and 23:00–24:00	0.02
Ordinary time	Remaining time	0.07

The wind power output curve, photovoltaic power output curve, electric load curve, and heat load curve of the grid-connected intelligent integrated energy system in Tayuanzhuang, Hebei Province are shown in Figure 2, based on a typical winter operation day.

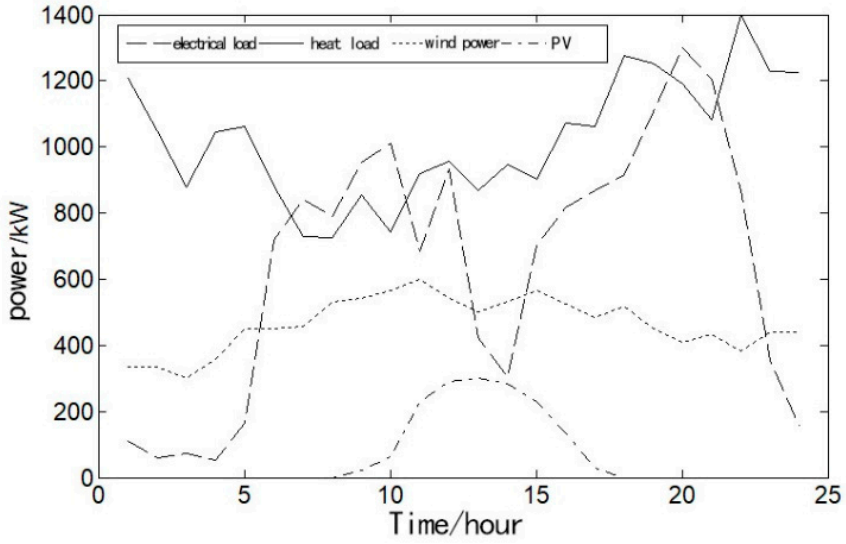

Figure 2. Wind power output, photovoltaic power output, and power curve of electric load and heat load on a typical winter operating day.

Taking a typical winter operation day with a large heating demand as an example, this paper developed two scenarios for optimizing economic dispatch of integrated energy systems; one was that the integrated energy system ran in the off-grid mode, the other was that the integrated energy system ran in the grid-connected mode.

The established model was run in order to obtain the optimized economic dispatch plan of the system under scenario 1 and scenario 2, as shown in Figures 3 and 4, respectively.

As can be seen from Figure 3, the charging and discharging of energy storage in the power subnet were frequent, and the charging and discharging states of energy storage were not determined by the time-sharing price level of the external network, as it was in the grid-connected mode. In order to meet the demands of both electric and thermal loads, the combined cooling, heating, and power microcombustor had basically reached full capacity in each period. The fuel cell output was also high

and was not limited to the peak load period. In each period, the interruptible load power of the system was high, and the power balance constraint was satisfied by abandoning part of the load power supply.

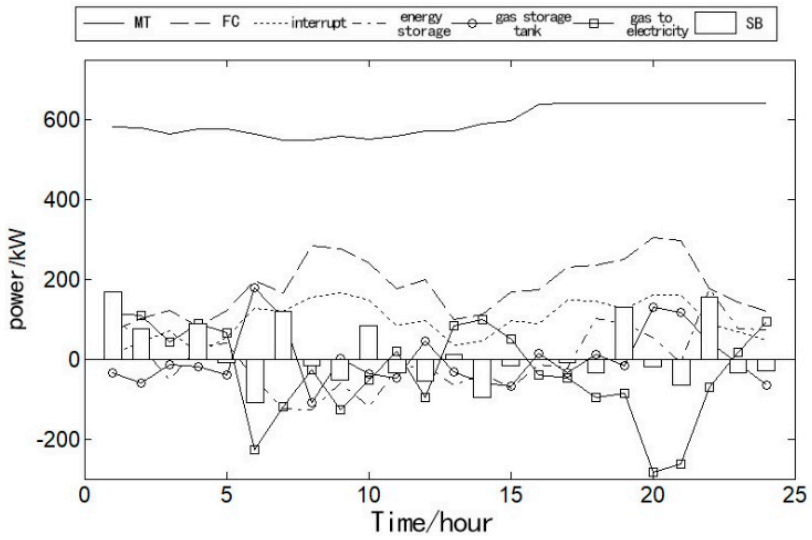

Figure 3. Optimizing economic dispatch scheme for integrated energy system in scenario 1.

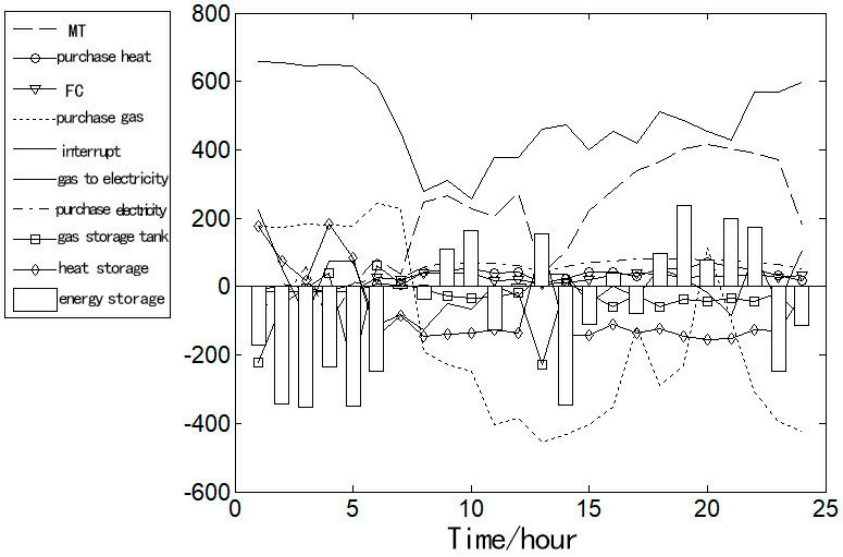

Figure 4. Optimizing economic dispatch scheme for integrated energy system in scenario 2.

As can be seen from Figure 4, the capacity of various energy supply modes in the integrated energy system was relatively high, which can meet the energy demands of each energy subnetwork. From the first period to the seventh period, due to the low level of time-sharing electricity price in the external network, the system received electricity from the external network exclusively, while the energy storage was in the charging state, which lays the foundation for peak cutting and valley filling in the following period. At this time, the heating load level of the energy interconnected microgrid was relatively high, and the system mainly met the demand by receiving heat from the external network. In this case, the combined cooling, heating and power units were used for heating. As a result, the cost of the electricity generated was not very economical compared to the time-sharing price of the external network, hence the system was not supplied predominantly by the combined cooling, heating, and power units. From the eighth to the thirteenth period, the power subnet entered the first peak load period, energy storage was discharged, and both the combined cooling, heating, and power microcombustion engine and fuel cells increased their output to meet the demand of the power load.

At this time, the amount of heat power that the system received from the outside network significantly declined. On the one hand, the level of heat load decreased at this time, while the demand of the system to receive heat from the outside network decreased with an increasing output of the CCHP units. Furthermore, because of the high time-sharing electricity prices in the outside network, it is more economical to replace the output of CCHP units to purchase electricity from the outside network and provide heating at the same time. From the fourteenth to the sixteenth period, the power subnet was at a low load, and the time-sharing price became low, at which time the energy storage re-entered the charging state. After the seventeenth period, the interconnected energy microgrid entered the second peak load period of the electric and thermal loads, at which time the operation characteristics were similar to those of the eighth to thirteenth period.

It can be seen from Table 3 that in the operation of scenario 1, the average integrated operating cost of the system was USD 1568.32, which was much larger than the average integrated operating cost of scenario 2. From this, it can be seen that the operating cost of the integrated energy system in the grid-connected operating mode were significantly lower than the operating costs in the off-grid operating modes. In actual operation, because the energy storage system was only charged at night, discharged during the day, and no charging activity was performed when the power was exhausted, the average comprehensive operating cost of the system in the grid-connected mode was relatively high.

Table 3. Average integrated operating cost in different modes.

Off-Grid Mode	Grid-Connected Mode	Actual Grid-Connected Mode
Average Integrated Operating Cost (USD)		
1568.32	1145.22	1584.88

In order to verify the effectiveness of the NSGA-II multiobjective function solving algorithm based on tent map chaotic optimization in solving the optimal economic dispatch model of an integrated energy system, particle swarm optimization was used to improve the artificial fish swarm algorithm, and the NSGA-II multiobjective function solving algorithm based on tent map chaotic optimization was used to solve the model 20 times. The average solution index was then compared, as shown in Table 4.

Table 4. Comparisons of solving indicators of integrated energy system optimal economic dispatch model based on three algorithms.

Model Solving Algorithm	Particle Swarm Optimization	Improved Artificial Fish Swarm Algorithm	NSGA-II Multiobjective Function Solving Algorithm Based on Tent Mapping Chaos Optimization	Reduced Percentage
Average integrated operating cost (USD)				
Scene 1	1633.27	1580.35	1568.32	3.98%
Scene 2	1183.37	1164.01	1145.22	3.22%
Average model solution time (s)				
Scene 1	23.64	19.62	16.67	29.48%
Scene 2	22.51	18.54	17.31	23.10%
Integrated operating cost standard deviation (USD)				
Scenario 1	9.77	7.67	6.74	31.01%
Scenario 2	10.91	9.47	7.87	27.86%

It can be seen from Table 4 that the improved artificial fish swarm algorithm was much faster at solving than the basic particle swarm algorithm, and the NSGA-II multiobjective function algorithm based on tent map chaos optimization used in this paper was faster than the basic particle swarm

algorithm in terms of solving speed—it was at least 23.10% faster and was more effective. In two different scenarios, with the shortening of the optimization time, the average comprehensive operating cost of the integrated energy system scheduling decreased from USD 1633.27 to USD 1568.32—a decrease of at least 3.22%—and its corresponding standard deviation also decreased by at least 27.86%.

In fact, the convergence curves of the NSGA-II multiobjective function solving algorithm based on tent map chaos optimization are shown in Figure 5 when Scenarios 1 and 2 were solved, respectively.

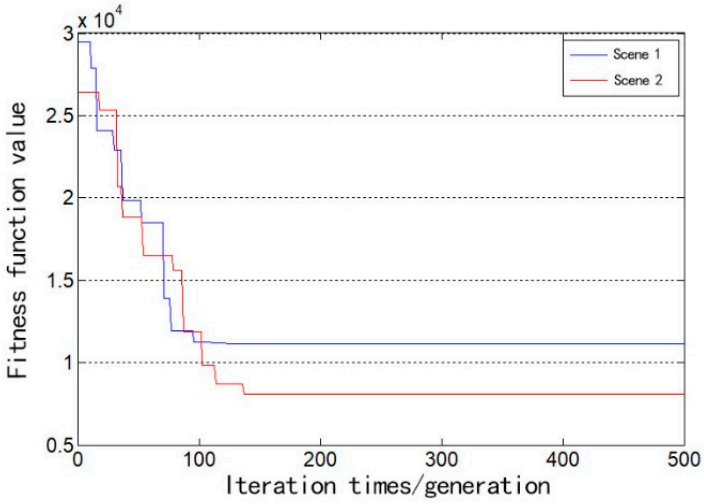

Figure 5. Scenario 1 and scenario 2 convergence curves of the NSGA-II multiobjective function solving algorithm based on tent mapping chaos optimization.

5. Conclusions

(1) Based on the multienergy complementary characteristics of the integrated energy system, this paper established an optimized economic dispatch model, and improved the NSGA-II algorithm based on the tent mapping chaos optimization algorithm to achieve a multiobjective model solution. The improved NSGA-II algorithm could be used in the algorithm to improve the solution efficiency in the early stage, which weakened the advantage of the elite solution in the later stage of the algorithm, and improved the possibility of the algorithm escaping the local optimum and continuing to optimize in a larger space.

(2) A simulation example for the demonstration project of Hebei Tayuanzhuang Smart Integrated Energy System demonstrated that the model established in this paper could formulate a multienergy complementary coordination plan between different forms of energy and fully reduce the system's energy supply cost. The comprehensive operating cost of the system in the off-grid operation mode in scenario 1 was significantly higher than that in the off-grid operation mode in scenario 1. This paper used the tent mapping chaos optimization algorithm to optimize the NSGA-II algorithm for the integrated energy system economic scheduling model, demonstrating that compared to the particle swarm algorithm and improved artificial fish swarm algorithm, it had better performance.

Author Contributions: S.C. designs the overall structure of the article, analyzed and interpreted the data results, and carefully revised the manuscript. S.W. collects data and calculates, writes relevant chapters of the article, integrates typesetting of the article, and draws tables. All authors have read and agreed to the published version of the manuscript.

Funding: This research was funded by the National Natural Science Foundation of China, grant number (71601078), the China Southern Power Grid Corporation Informatization Key Project, grant number (031900HK42180010).

Conflicts of Interest: The authors declare no conflict of interest.

References

1. Liu, C.; Shahidehpour, M.; Wang, J. Application of augmented lagrangian relaxation to coordinated scheduling of interdependent hydrothermal power and natural gas systems. *IET Gener. Transm. Distrib.* **2010**, *4*, 1314–1325. [CrossRef]
2. Zhang, X.; Shahidehpour, M.; Alabdulwahab, A.; Abusorrah, A. Hourly electricity demand response in the stochastic day-ahead sched-uling of coordinated electricity and natural gas networks. *IEEE Trans. Power Syst.* **2015**, *31*, 1–10.
3. Jia, H.; Mu, Y.; Yu, X. Thought about the Integrated Energy System in China. *Power Constr.* **2015**, *36*, 16–25.
4. Wang, W.; Wang, D.; Jia, H.; Chen, Z.; Guo, B.Q.; Zhou, H.M.; Fang, M.W. Steady State Analysis of Electricity-Gas Regional Integrated Energy System With Consideration of NGS Network Status. *China J. Electr. Eng.* **2017**, *37*, 1293–1304.
5. Yu, X.; Xu, X.; Chen, S.; Wu, J.; Jia, H. A Brief Review to Integrated Energy System and Energy Internet. *J. Electr. Technol.* **2016**, *31*, 1–13.
6. Yu, B.; Wu, L.; Lu, X. Optimal Dispatching Method of Integrated Community Energy System. *Power Constr.* **2016**, *37*, 70–76.
7. Gu, W.; Lu, S.; Wang, J.; Yin, X.; Zhang, C.L.; Wang, Z.H. Modeling of the Heating Network for Multi-district Integrated Energy System and Its Operation Optimization. *J. Electr. Eng. China* **2017**, *37*, 1305–1315.
8. Shi, J.; Xu, J.; Zeng, B.; Zhang, J. A Bi-Level Optimal Operation for Energy Hub Based on Regulating Heat-to-Electric Ratio Mode. *Power Grid Technol.* **2016**, *40*, 2959–2966.
9. Lu, Z.; Yang, Y.; Geng, L.; Pan, L.; He, L.; Li, X. Low-carbon Economic Dispatch of the Integrated Electrical and Heating Systems Based on Benders Decomposition. *J. Electr. Eng. China* **2018**, *38*, 1922–1934.
10. Zhou, C.H.; Zheng, J.H.; Jing, Z.X.; Wu, Q.; Zhou, X. Multi-Objective Optimal Design of Integrated Energy System for Park-Level Microgrid. *Power Grid Technol.* **2018**, *42*, 1687–1697.
11. Zhang, X.; Tang, Q.; Yan, W.; Wei, J.F.; Hou, K.; Wang, Y.; He, Z. Reliability Evaluation of Integrated Community Energy System Based on Particle-Swarm-Interior-Point Hybrid Optimization Al-gorithm. *Power Constr.* **2017**, *38*, 104–111.
12. Lin, W.; Jin, X.; Mu, Y.; Jia, H.; Xu, X.; Yu, X. Multi-objective Optimal Hybrid Power Flow Algorithm for Integrated Local Area Energy System. *China J. Electr. Eng.* **2017**, *37*, 5829–5839.
13. Deb, K.; Pratap, A.; Agarwal, S.; Meyarivan, T.A.M.T. A fast and elitist multi-objective genetic algorithms: NSGA-II. *IEEE Trans. Evol. Comput.* **2002**, *6*, 182–197. [CrossRef]
14. Wang, S.X.; Jiang, Y.; Han, F.A. Chaotic Optimization Strategy Used in Parameter Identification of Composite Load Model. *China J. Electr. Eng.* **2006**, *26*, 111–116.
15. Shan, L.; Qiang, H.; Li, J.; Wang, Z.Q. Chaotic optimization algorithm based on Tent map. *Control Decis. Mak.* **2005**, *20*, 179–182.
16. Zheng, X.W.; Li, Y.; Liu, H.; Duan, H.C. A study on a cooperative character modeling based on an improved NSGA II. *Multimed. Tools Appl.* **2016**, *75*, 4305–4320. [CrossRef]
17. Li, J.; Yang, L.; Liu, J.L.; Yang, D.L.; Zhang, C. Multi-objective reactive power optimization based on adaptive chaotic particle swarm optimization. *Power Syst. Prot. Control* **2011**, *39*, 26–31.